Int. J. Heat Mass Transfer. Vol. 26, No. 11, pp. 1669–1677, 1983
Printed in Great Britain

0017-9310/83 $3.00 + 0.00
Pergamon Press Ltd.

LAMINAR FREE CONVECTION AROUND HORIZONTAL CIRCULAR CYLINDERS

LUCIANO M. DE SOCIO
Institute of Applied Mechanics, Polytechnic of Turin, Corso Duca degli Abruzzi, 24-Turin 10129, Italy

(*Received* 8 *November* 1982)

Abstract—Two series of experiments were performed in order to measure the average and the local heat transfer coefficients in laminar natural convection around horizontal circular cylinders, whose surface was in part isothermal and in part adiabatic. Correlations of data are presented and comparisons with the results of the integral solution of the corresponding boundary layer equations are given. Visual observations of some characteristics of the flow regions were also carried out and some of their main aspects are discussed.

NOMENCLATURE

c_p	specific heat at constant pressure
D	diameter of the cylinder
g	acceleration of gravity
Gr	Grashof number, Ra/Pr
h	local heat transfer coefficient
$\bar{h}$	average heat transfer coefficient
k	thermal conductivity
L	length of the cylinder
Nu	local Nusselt number
$\overline{Nu}$	average Nusselt number, equation (4)
$\overline{Nu}^*$	average Nusselt number, equation (5)
Pr	Prandtl number, $c_p\mu/k$
r, θ	polar coordinates
Ra	Rayleigh number
t	dimensionless temperature difference, $(T-T_\infty)/(T_w-T_\infty)$
T	temperature
T_∞	temperature at infinity
ΔT_w	$T-T_w$
ΔT_{w0}	$T-T_{w0}$
u	dimensionless velocity, UD/ν
y	distance from the wall along r, dimensionless with respect to D

Greek symbols

β	thermal expansion coefficient
δ	boundary layer thickness, dimensionless with respect to D
μ	viscosity
ν	kinematic viscosity

Subscripts

w	value at the wall
w0	value at the wall in the isothermal region

INTRODUCTION

FREE convection around horizontal circular cylinders has been extensively investigated, both experimentally and analytically, in the basic situation corresponding to a constant temperature of the surface. Excellent reviews of the existing bibliography on this subject can be found in refs. [1–3]. To the author's knowledge, however, no attention has so far been paid to other thermal conditions of noticeable practical interest, as are those relative to partly isothermal and partly adiabatic cylindrical surfaces.

In engineering, situations related to the last ones described above occur, for example, in heat transfer around metallic tubes partially covered by snow or ice or around pipes where an internal layer of deposited salt greatly decreases—in some areas of the cylinders—the heat conducted through the wall.

This paper deals with the plane problem of laminar natural convection around horizontal circular cylinders, the external surfaces of which are everywhere isothermal, with the exception of a region of variable extent which is adiabatic. Furthermore, it seemed worthwhile to determine some aspects of the local heat transfer coefficient distribution, to evaluate the greater effectiveness of the region around the forward stagnation point (as far as the Nusselt number is concerned) with respect to the rest of the surface. Numerical and experimental data on the local heat transfer coefficient have been given for the isothermal case in ref. [4].

A sketch of the investigated situation is shown in Fig. 1, where, in particular, the adiabatic sector corresponding to an angle 2ϕ is symmetric with respect to the vertical diameter, whereas the length of the relative arc is l. In the experiments, l could be reduced to zero, in so restoring the fully isothermal situation.

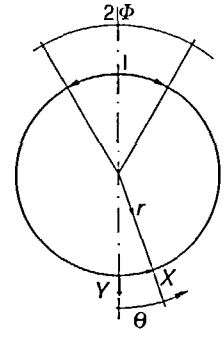

FIG. 1. Geometry of the problem.

Two series of experiments were performed. The first one was relative to measurements of the average heat transfer coefficient around three cylinders, where the isothermal regions corresponded to 360°, 270° and 180°, respectively. In the second experimental rig, the local Nusselt number was measured around a cylinder whose surface was isothermal for 180° and insulated for the remaining 180°. After the experimental results for the fully isothermal cylinder were compared with the existing data, with excellent agreement, the influence of the extension of the adiabatic sector on the average heat transfer was evaluated and the correlation for this set of data is presented.

In the first series of experiments, the heat transfer rates were evaluated by measuring the electric power dissipation from the models. The results obtained by adopting the second experimental apparatus were obtained by means of a Wollaston bi-prism interferometer and using Schlieren and shadowgraph techniques. By these systems, in addition to the determination of the local heat transfer, it was possible to carry out an observation of some characteristics of the boundary layer and of the plume leaving the model.

A simple integral approach was finally used for the analysis of the boundary layer around the half adiabatic–half isothermal cylinder and the results were compared with the experimental data and with the theoretical computation of previous authors.

THE FIRST SET OF EXPERIMENTS

Description and results

Measurements of the average heat transfer coefficients were carried out on three models. Three hollow cylinders of 37 mm O.D. and 15 mm I.D. were machined from aluminum rods. The common length of the models was 0.5 m. In two cylinders, angular sectors of 2ϕ equal to 90° and 180°, respectively, were removed and substituted by identical Teflon sectors which were accurately fastened to the metal surfaces by an epoxy resin. The final models were painted dull black.

Heating elements of shielded Ni–Cr wire of diameter 0.2 mm were located in the cavities indented in ceramic rods of stellar cross section which, in turn, were set inside the models for support.

The Ni–Cr elements (eight, six and four of them, respectively, for the three models, a decreasing number of resistors corresponding to an increasing l) could be independently electrically heated by stabilized AC power and the total power was measured by means of a wattmeter with a maximum error of $\pm 0.01\%$ on the full-scale reading of 500 W.

Twenty copper–constantan J shielded thermocouples of 0.2 mm O.D. were adopted for temperature monitoring at locations drilled up to 0.1 mm from the surfaces. In particular, five cross sections were instrumented at 10, 12, 250, 375, and 490 mm along the axis of the cylinders, whereas four thermocouples were angularly distributed around the circumference of the cross section. The four thermocouples in each section were displaced only in the metallic portion of the models, with the exception of one thermocouple in the Teflon region in the central section.

The readings of the thermocouples were taken by means of a multimeter with a maximum error of $\pm 1\,\mu$V, on the set of measurements.

During the experiments, the models were situated between two windows of optical glass, 60 cm in diameter, located in two 4×4 m vertical walls of bakelite, in order to provide two-dimensional flow conditions and to prevent perturbing effects from the external ambient. Bakelite discs of thickness 5 mm were added to thermally insulate the ends of the models.

The entire apparatus was located in a room of practically constant thermal characteristics corresponding to an average Prandtl number of 0.733. The models were installed at a distance of 2.5 m from the ceiling of the room and 2 m from the floor. During each run an average time span of about 5 h elapsed after the electric power was supplied to the model and before collecting the experimental data in order to ensure steady flow and thermal conditions.

In addition to the heat transfer experiment, the models were also placed in the beam of a Wollaston prism–Schlieren interferometer, providing some qualitative results on the plume and a check of the laminar regime.

In particular the interferometric device adopted a He–Ne polarized laser source of 15 mW, a beam expander, two spherical mirrors 30 cm in diameter and with a focal length of 3 m, a Wollaston quartz bi-prism with a divergence angle of 5′, a polarizer and a semi-transparent glass screen. For the general characteristics of a Wollaston prism–Schlieren interferometer and the resulting data reduction see ref. [5].

The experiments were performed in the range of Rayleigh numbers, Ra, from 1.5×10^4 to 6×10^5, with

$$Ra = Pr\ Gr = Pr \frac{g}{\nu^2} \beta (T_{w0} - T_\infty) D^3, \qquad (1)$$

where Gr is the Grashof number and the rest of the symbols are defined in the Nomenclature. The values of the physical properties appearing in equation (1) were evaluated at the film temperature given by $T_f = \frac{1}{2}(T_{w0} + T_\infty)$, where T_{w0} is the wall temperature of the isothermal part of the model and T_∞ is the temperature at infinity.

The average heat transfer coefficient $\bar{h}$ was calculated from

$$\bar{h} = \frac{Q}{S(T_{w0} - T_\infty)} = \frac{Q_e - Q_r}{S(T_{w0} - T_\infty)}, \qquad (2)$$

where Q is the net heat power transferred by convection, Q_e is the electric power supplied to the heating elements, and Q_r is the radiation power evaluated by the expression

$$Q_r = \varepsilon \sigma (T_{w0}^4 - T_0^4) S. \qquad (3)$$

In equations (2) and (3) S is equal to the heated part of the surface of the cylinder, σ is the Stefan–Boltzmann

constant, and ε is the surface emissivity equal to 0.97 for dull black enamel.

Actually, when equation (3) is applied, the dissipation by radiation from the insulated part of the cylinder is not considered. However, the error is negligible in the considered situations.

Two different definitions of the average Nusselt number will be considered

$$\overline{Nu} = \frac{\bar{h}D}{k} = \frac{Q_c - Q_r}{k(T_w - T_\infty)} \frac{1}{e\pi L}, \tag{4}$$

$$\overline{Nu}^* = \frac{\bar{h}e\pi D}{k} = \frac{Q_c - Q_r}{k(T_w - T_\infty)L}, \tag{5}$$

where e is the percentage of the total surface of the cylinder which is kept isothermal. Equation (4) corresponds to considering the heat flux relative to only that part of the surface which is actually kept at T_{w0}. In this sense a comparison, at given Ra and Pr, of the values of $\overline{Nu}$ for the various geometries enables the relative efficiency of models with different heated portions to be evaluated.

When $\overline{Nu}^*$ is considered, the presence to different extents of the insulated regions penalizes the global heat transfer for models which are not completely isothermal.

Figure 2 presents the experimental results for the isothermal cylinder and the empirical correlations proposed by several authors. The data obtained are well situated among the results of other authors and are in excellent agreement with those of refs. [7–11]. Note

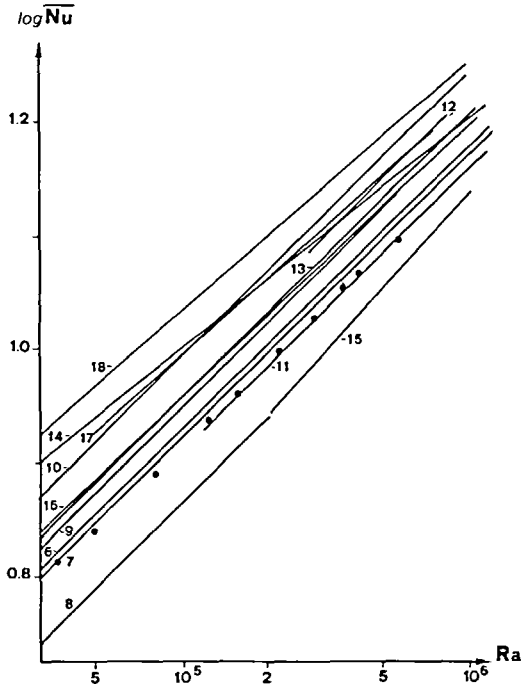

FIG. 2. Isothermal cylinders. The lines represent proposed empirical correlations. Numbers indicate references at the end of the paper; dots are results of the present work.

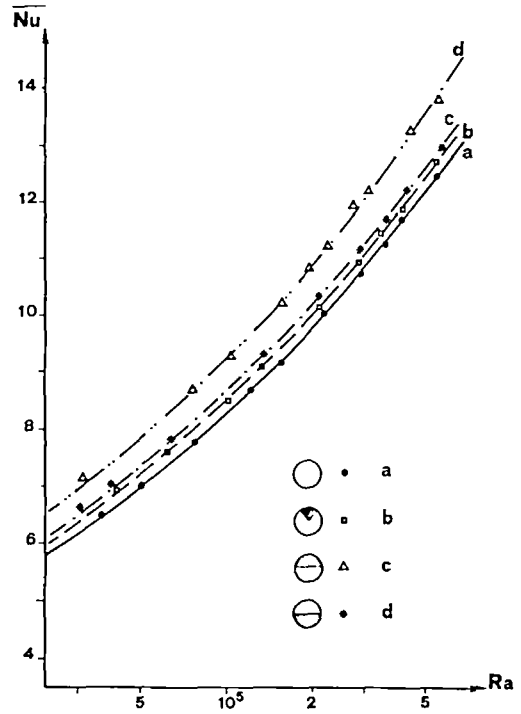

FIG. 3. Experimental results for the four examined cases. The lines represent the proposed correlations.

that, in the present experiment, the aspect ratio L/D was equal to about 13.5 and the space ratio L_∞/D was 67.6, where L_∞ is the height of the test room. In the data of refs. [7–11] both the aspect ratios and the space ratios were quite high, whereas in most of the other researches these two ratios were in general not that high.

With this in mind the experimental results obtained on the isothermal cylinder can be considered accurate.

Figure 3 shows the results for all the four configurations which have been investigated: three of them correspond to a forward stagnation point coincident with the middle point of the heated region, whereas in the fourth case, for $\phi = 90°$, this middle point is the backward stagnation point.

For each set of experimental data, a correlation formula of the kind

$$\overline{Nu} = B\, Ra^m, \tag{6}$$

has been evaluated and a least square interpolation leads to the values reported in Table 1.

In Table 1 the coefficients appearing in the analogous

Table 1

ϕ (deg.)	Line in Fig. 3	B	m	B^*
0	a	0.488	0.246	1.533
45	b	0.543	0.239	1.280
90	c	0.581	0.241	0.912
90	d	0.569	0.236	0.894

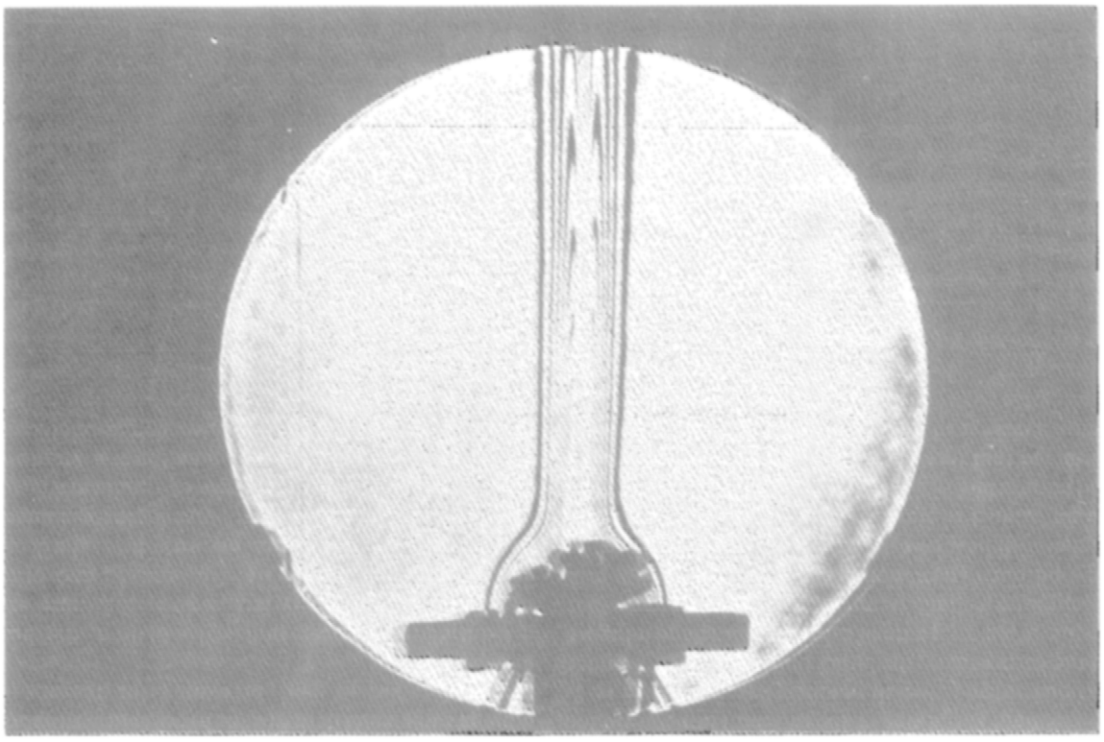

FIG. 4. Infinite distance fringes of a Woolaston bi-prism–Schlieren interferometric picture at $Pr = 0.733$ and $Gr = 3 \times 10^5$.

correlation

$$\overline{Nu^*} = B^* \, Ra^m, \tag{7}$$

are also given. Of course, the exponent of Ra in equations (6) and (7) are equal. The empirical correlations (6) for the various cases are drawn as lines a–d in Fig. 3.

A comparison of the coefficients B^* shows the increase of the total heat transferred with the increasing heated surface. The values of B^* for the two reversed cases, c and d, on the other hand, reveals the greater efficiency of a heated forward stagnation point.

If the comparison is done on the values of B, then the average Nusselt number $\overline{Nu}$ increases from $\phi = 0°$ to 90° confirming that the region around the forward stagnation point is the most efficient as far as the heat transfer is concerned. The fact that the surface about the rear stagnation point is still quite active from the point of view of the heat dissipation is shown by the value of B for case d when compared with cases a–c. However, one should note the drop in heat transfer when passing from case c to d. The entire visualized field, for about five diameters of the cylinder, showed a perfectly laminar plume leading the models during all the experiments. Figure 4 corresponds to a picture taken at $Gr = 3.2 \times 10^5$ by the Wollaston prism–Schlieren interferometer, for fringes at infinite distance. Note in the foreground the double images of the objects, supporting arms and connecting cables. The outermost fringe indicates the limits of the boundary layer around the cylinder and of the plume.

THE SECOND SET OF EXPERIMENTS

Description and results

In the second part of this experimental investigation the distribution of the local Nusselt number, $Nu = h(0)D/k$ was measured around a cylinder with a diameter of 150 mm and a length of 600 mm ($L/D = 4$).

The isothermal part of the surface corresponds to $2\phi = 180°$ and was realized by means of a semicircular copper tile, 1 cm thick, while the rest of the cylindrical model was made of aged oak wood. At the ends of the model two discs of wood, 3 cm thick were placed for the purpose of insulation, and in order to fasten together the copper tile and the wood. The end discs were joined by two horizontal steel arms for support and for the passage of thermocouples and electric wires. In correspondence with the metal part 12 spatially distributed grooves were machined in the wooden support in the axial direction and in them 12 elements of shielded 0.2 mm Ni–Cr wire were placed adjacent to the copper tile and insulated from the walls of the grooves by means of rockwool.

The heating elements could be separately connected to the same power supply adopted in the first experiment.

Twelve copper–constantan J thermocouples, 0.2 mm O.D., were soldered to the metal part of the model in holes drilled up to 0.1 mm from the external surface. The thermocouples were angularly distributed in four sections of the model at 1, 20, 40, and 49 cm, respectively, along the axis of the cylinder, at $\theta = \pm 42°$

and 0°. A probe mounting a shielded J thermocouple 0.2 mm in diameter could be moved along the surface of the insulated region for measurements of the local temperature.

The model, painted dull black, was situated between two windows of optical glass, 60 cm O.D., opened in two 4 × 4 m vertical bakelite walls. The model could be vertically moved about 10 cm around a position 2.5 m from the ceiling of the room ($L_\infty/D \cong 16.7$) in the beam of the Wollaston bi-prism interferometer.

Figure 5 shows the similarity parameter $Nu/Gr^{0.25}$, at $Pr = 0.733$, vs the angle θ, for two series of measurements at different Grashof numbers. The result of a simple integral solution of the boundary layer equations (see the Appendix) is also shown in Fig. 5. The discrepancies between the theoretical curve and the experimental data can be ascribed to (a) errors in the interferometric measurements (up to 13% in evaluation of the local heat flux) due to the large number of intervening variables, and (b) the inadequacy of the theoretical model, which involves a discontinuous variation of the heat flux at $\theta = 90°$, whereas there is still some measured heat transfer rate up to $\theta = 107°$ and which, more important, involves a prediction of the boundary layer thickness at the stagnation point. However, this inadequacy in the prediction of the heat transfer rate is common to other more sophisticated procedures, as the local non-similarity treatment of Muntasser and Mulligan which, at $\theta = 0°$, predict $Nu(0)/Gr^{0.25} = 0.448$ [19].

Figure 6 shows experimental data and theoretical predictions, by the integral method, concerning the temperature distribution at the wall and the thickness of the boundary layer, δ. This thickness was measured by assuming for it, in the interferometric images, the distance from the wall where the deviation of the fringes is negligible. Figure 7 shows an interferometric picture adopted for these measurements.

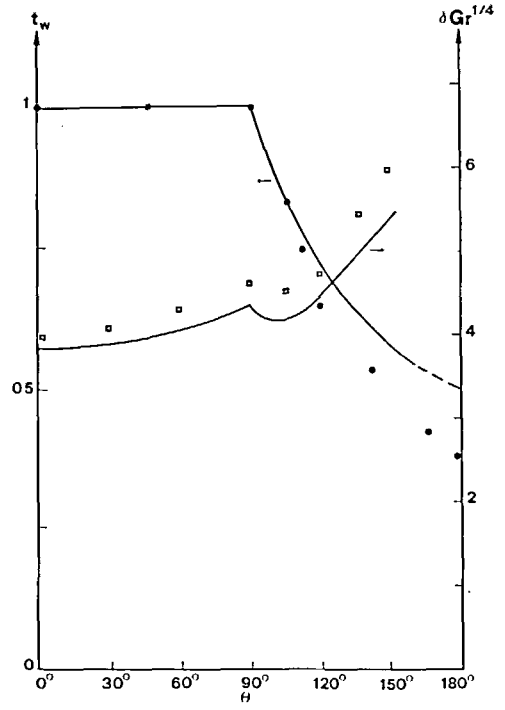

FIG. 6. Temperature distribution at the wall ϕ, ●, experimental data; solid line, theoretical prediction. Also, boundary layer thickness parameter vs θ. ■, experimental data; continuous line, solution of the integral boundary layer equations.

A relevant problem regarding the natural convection around cylinders concerns the angle at which separation occurs. Assuming for this angle the value of θ wherefrom the outermost limit line of the boundary layer (fringes at infinite distance) becomes thicker and thicker, changes its curvature and becomes aligned with the plume, one measured values between 155° and 160° for $Gr = 9.03 \times 10^6$ and 13.01×10^6, respectively.

Figure 8 shows an interferometric picture for fringes at infinite distance used for these calculations. The angle of separation is somehow smaller than the corresponding angle for a fully isothermal cylinder (about 165°). Finally it is interesting to observe the two Schlieren pictures of Figs. 9(a) and (b). They represent the trailing edge of the system and were obtained with the knife first horizontal and then vertical, and are, in some respect, complementary.

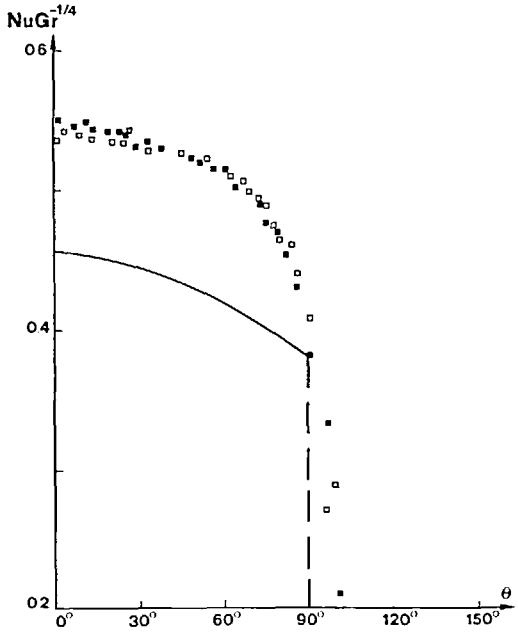

FIG. 5. Experimental data and theoretical prediction of the heat transfer rate vs θ. □, $Gr = 9.03 \times 10^6$; ■, $Gr = 13.01 \times 10^6$. $Pr = 0.733$.

Acknowledgement—This work was supported in part by the Italian National Research Council (CNR) through Grant No. 81.02447.07.

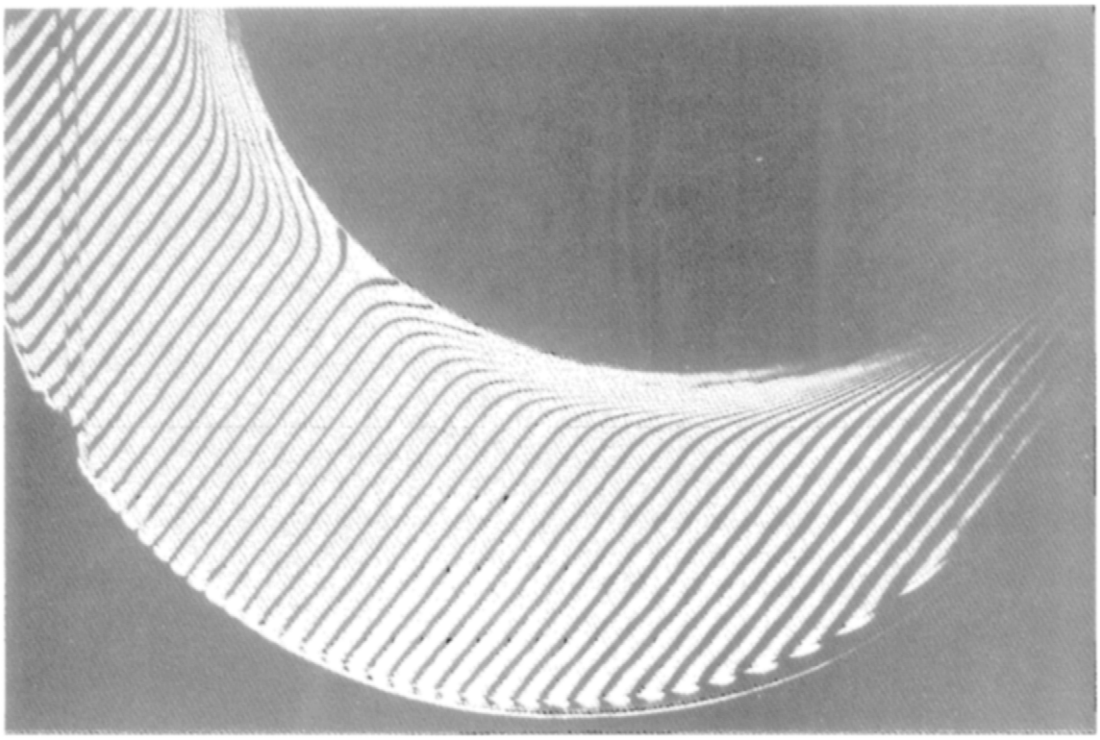

FIG. 7. Interferometric picture of the region around the stagnation point: $Pr = 0.733$, $Gr = 2 \times 10^7$.

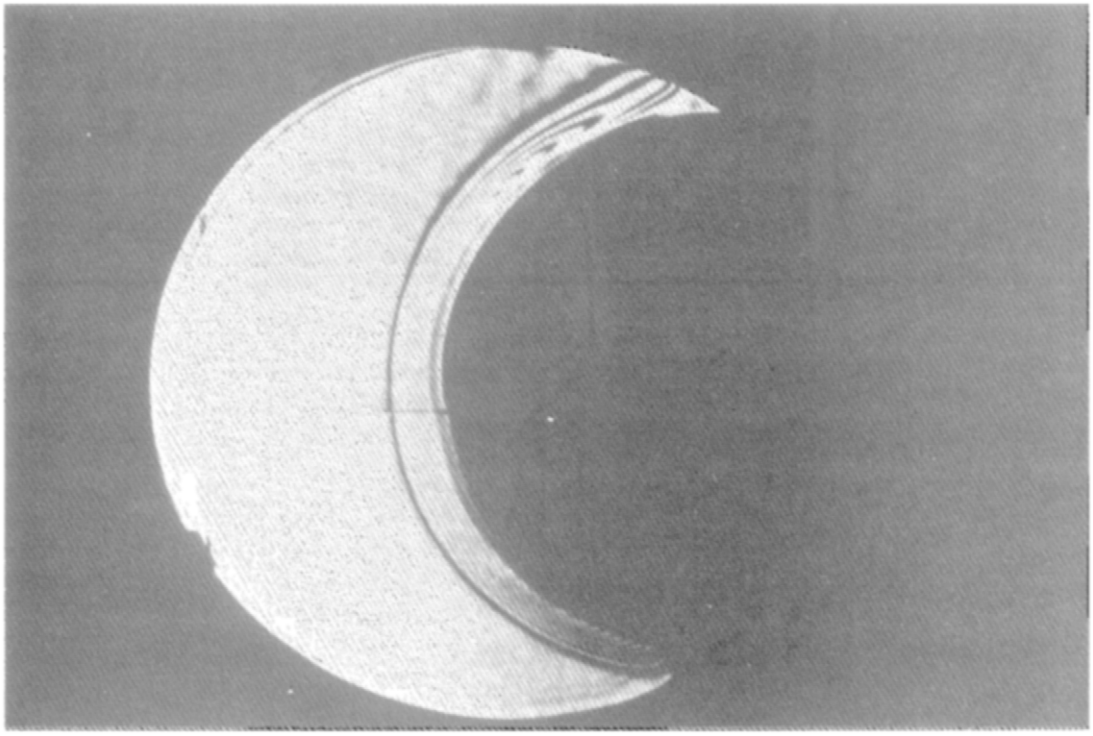

FIG. 8. Fringes at infinite distance for $Gr = 9.03 \times 10^6$ at $Pr = 0.733$. The bi-prism is in the focus of the second mirror and the optical axis is vertical. The fringes correspond to isotherms.

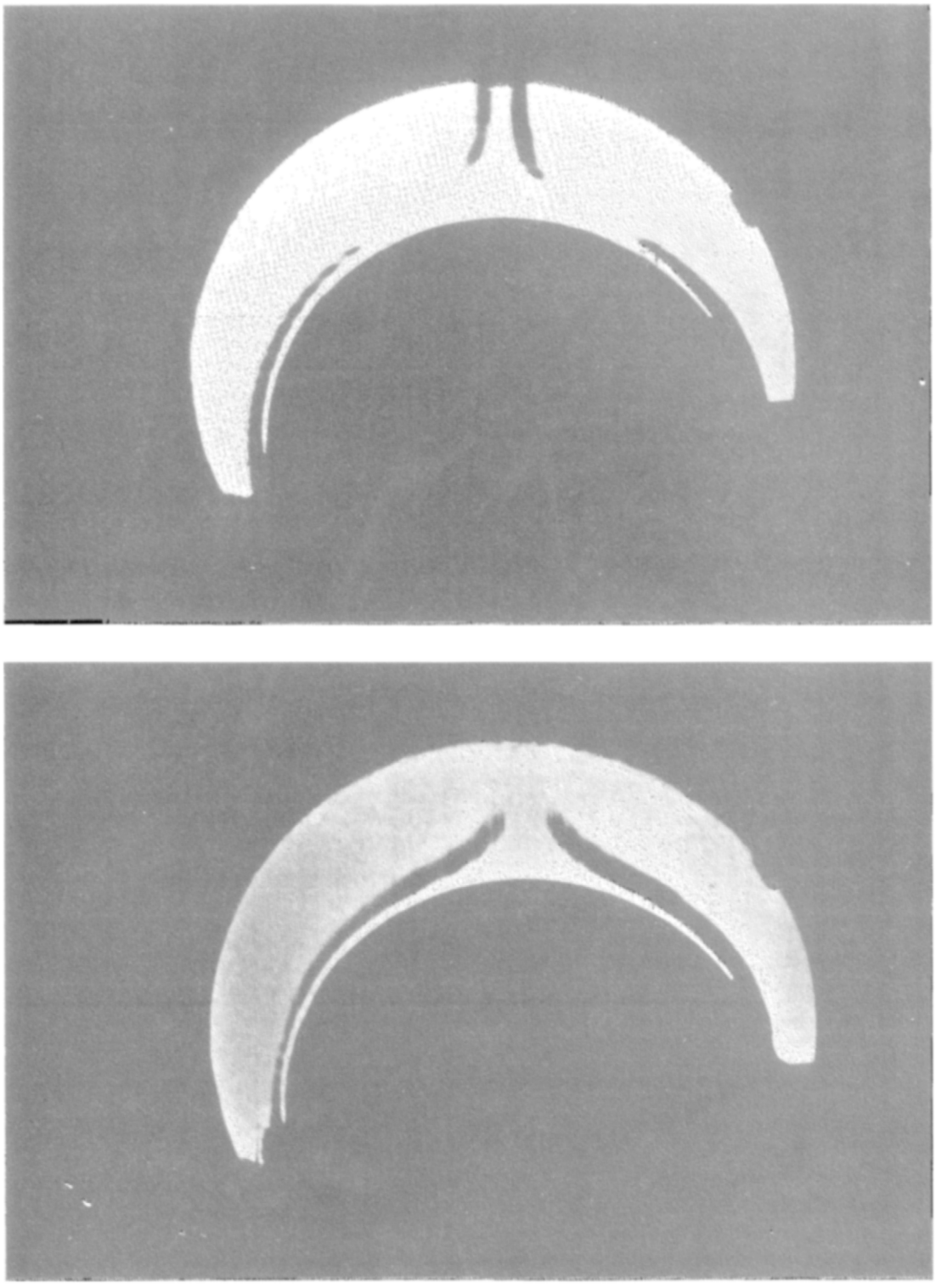

FIG. 9. Schlieren pictures of the model at $Pr = 0.733$ and $Gr = 5.3 \times 10^7$. Top: horizontal knife; bottom: vertical knife.

REFERENCES

1. B. Gebhart, Natural convection flows and stability, *Adv. Heat Transfer* **9**, 273–346 (1973).
2. V. T. Morgan, The overall convective heat transfer for smooth circular cylinders, *Adv. Heat Transfer* **11**, 199–264 (1975).
3. Y. Jaluria, Natural convection. Heat and mass transfer, *Heat Mass Transfer* **5** (1980).
4. T. H. Kuehn and R. J. Goldstein, Numerical solution of the Stokes–Navier equations for laminar natural convection about a horizontal isothermal circular cylinder, *Int. J. Heat Mass Transfer* **23**, 971–979 (1980).
5. V. Sernas, The Wollaston prism Schlieren interferometer, The von Kármàn Inst. for Fluid Dyn., Rhôde Saint Génèse, Lecture Series 96 (1977).
6. F. Wamsler, Die Wärmeabgabe geheizter Körper an Luft, *VDI ForschHft.* No. 98/99 (1911).
7. A. H. Davis, The cooling power of a stream of viscous fluid, *Phil. Mag.* **44**, 940–944 (1922).
8. W. Koch, Über die Wärmeabgabe geheizter Rohre bei verschiedener Neigung der Rohrachse, *Gesundh.-Ing. Beih.*, Ser. 1, **22**(1), 1–29 (1927).
9. K. Jodlbauer, Das Temperatur- und Geschwindigkeitsfeld um ein geheiztes Rohr bei freier Konvektion, *Forsch. Geb. IngWes.* **4**, 157–172 (1933).
10. M. Jakob and W. Linke, Der Wärmeübergang beim Verdampfen von Flüssigkeiten an senkrechten und waagerechten Fläschen, *Phys. Z.* **36**, 267–280 (1935).
11. G. A. Etemad, Free-convection heat transfer from a rotating horizontal cylinder to ambient air with interferometric study of flow, *Trans. Am. Soc. Mech. Engrs* **77**, 1283–1289 (1955).
12. W. M. Kays and I. S. Bjorklund, Heat transfer from a rotating cylinder with and without crossflow, *Trans. Am. Soc. Mech. Engrs* **80**, 70–78 (1958).
13. A. A. Zhukauskas, A. A. Shlanchyauskas and E. P. Yaronis, Effect of ultrasonic waves on heat transfer of bodies in liquids, *Inzh.-Fiz. Zh.* **4**(1), 58–62 (1961).
14. C. W. Rice, Free and forces convection of heat in cases and liquids, *Trans. Am. Inst. Elec. Engrs* **42**, 653–701 (1923).
15. W. Koch, Über die Wärmeabgabe geheizter Rohre bei verschiedener Neigung der Rohrachse, *Gesundh.-Ing. Beih.*, Ser. 1, **22**,(2), 1–29 (1927).
16. O. R. Schurig and C. W. Frick, Heating and current carrying capacity of bare conductors for outdoor service, *Gen. Elect. Rev.* **33**, 141–157 (1950).
17. W. E. Mason and L. M. K. Boelter, Vibration—its effect on heat transfer, *Pwr Pl. Engng* **44**, 43–44 (1940).
18. E. Weder, Messung des gleichzeitigen Wärme-und Stoffübergangs am horizontalen Zylinder bei freier Konvektion, *Wärme Stoffübertragung* **1**, 10–14 (1968).
19. M. A. Muntasser and J. C. Mulligan, A local non similarity analysis of free convection from a horizontal cylindrical surface, *J. Heat Transfer* **100**, 165–167 (1978).
20. H. J. Merk and J. A. Prins, Thermal convection in laminar boundary layers, I, II, *Appl. Scient. Res.* **A4**, 11–24 (1954); **4**, 195–206 (1954).

APPENDIX

AN INTEGRAL SOLUTION OF THE BOUNDARY LAYER EQUATIONS

An integral approach to the solution of the boundary layer equations for the free convection around isothermal circular horizontal cylinders has been followed by several authors. In this paper the integral form of the basic set of equations [1] will be solved by extending, to the non-completely isothermal case, the method of Merk and Prins ($Pr \cong 1$) [20].

For the present case, a third degree polynomial is assumed for the velocity profile and a fifth degree polynomial for the dimensionless temperature profile. In particular taking into account the proper boundary conditions, one puts $\eta = y/\delta$, and

$$u = Gr^{1/2} F(\xi)\eta(1-\eta^2),$$

$$t = t_0 + \lambda t_1,$$

where

$$t_0 = 1 - 10\eta^3 + 15\eta^4 - 6\eta^5,$$

$$t_1 = \eta - 6\eta^3 + 8\eta^4 - 3\eta^5$$

and $\lambda = (\mathrm{d}t/\mathrm{d}\eta)_w$ is equal to zero on the adiabatic surface and is unknown along the isothermal surface.

Taking into account that, at the wall, one has

$$\left.\frac{\mathrm{d}^3 t}{\mathrm{d}\eta^3}\right|_w = \left.\frac{\partial u}{\partial \eta}\right|_w \left.\frac{\mathrm{d}t}{\mathrm{d}\xi}\right|_w, \tag{A1}$$

it is possible to calculate $\lambda = -5/3$. Note that $Nu = -\lambda/\delta$.

Introducing the definition of a new function

$$G(\xi) = Gr^{-0.25}/\delta(\xi),$$

one finally has, from the integral equations for the isothermal region

$$\frac{\mathrm{d}F}{\mathrm{d}\theta} = \frac{35}{2}\frac{\sin\theta}{F} - \left(\frac{105}{2} + \frac{420}{17}\right)G^2,$$

$$\frac{\mathrm{d}G}{\mathrm{d}\theta} = \left[\frac{35}{2}\frac{\sin\theta}{F} - \left(\frac{105}{2} + \frac{2520}{21}\right)G^2\right]\left(\frac{G}{F}\right),$$

where for the angle θ the relation $\theta = 2\xi$ holds. This sytem can be easily solved by a simple numerical procedure, provided that the initial conditions at the forward stagnation point $\xi = 0$ are given. These conditions are obtained, following the same approach of ref. [20], by matching the integral solutions to the similar solutions, F_s and G_s, around $\theta = 0$, that is

$$F_s = k_1\theta,$$

$$G_s = k_2.$$

In the present case, $k_1 = 2.060$ and $k_2 = 0.289$.

Above the adiabatic wall the unknown functions are $F(\xi)$, $G(\xi)$ and t_w. The integral equations and equation (A1) provide

$$\frac{\mathrm{d}F}{\mathrm{d}\theta} = \frac{105}{4}\frac{\sin\theta}{F} - \left(\frac{105}{2+30}\right)G^2,$$

$$\frac{\mathrm{d}G}{\mathrm{d}\theta} = \left[\frac{105}{4}\frac{\sin\theta}{F} - \left(\frac{105}{2} + 60\right)G^2\right]\left(\frac{G}{F}\right),$$

$$\mathrm{d}E/\mathrm{d}\theta = -30\,EG^2/F,$$

with the initial conditions $E(0) = 1$, and $F(0)$ and $G(0)$ matching the solutions for the isothermal region.

CONVECTION NATURELLE LAMINAIRE AUTOUR DE CYLINDRES CIRCULAIRES HORIZONTAUX

Résumé—Deux séries de mesures sont conduites pour mesurer les coefficients de transfert thermique local et moyen en convection naturelle laminaire autour de cylindres circulaires horizontaux dont la surface est en partie isotherme et en partie adiabatique. Des formules empiriques sont présentées et des comparaisons sont faites avec les résultats de la solution intégrale des équations de la couche limite. Des observations visuelles de quelques caractéristiques de l'écoulement sont présentées et on discute certains de leurs aspects principaux.

LAMINARE FREIE KONVEKTION AN HORIZONTALEN KREISZYLINDERN

Zusammenfassung—Es wurden zwei Versuchsreihen durchgeführt, um die mittleren und die örtlichen Wärmeübergangskoeffizienten in laminarer freier Konvektion an horizontalen Kreiszylindern, deren Oberflächen dabei teils isotherm teils adiabat gehalten werden, zu messen. Auftragungen der Versuchsergebnisse werden präsentiert und mit den Ergebnissen der Lösung der entsprechenden Grenzschichtgleichungen nach der Integralmethode verglichen. Gleichfalls werden visuelle Beobachtungen einiger charakteristischer Erscheinungen der Strömungsgebiete durchgeführt und ihre wesentlichen Aspekte diskutiert.

ЛАМИНАРНАЯ СВОБОДНАЯ КОНВЕКЦИЯ ВОКРУГ ГОРИЗОНТАЛЬНЫХ КРУГОВЫХ ЦИЛИНДРОВ

Аннотация—Проведены две серии экспериментов по измерению средних и локальных коэффициентов теплопереноса при ламинарной естественной конвекции вокруг горизонтальных круговых цилиндров, поверхность которых является частично изотермической и частично адиабатической. Выведены обобщающие зависимости и проведено сравнение с результатами интегрального решения соответствующих уравнений пограничного слоя. Выполнены также визуальные наблюдения ряда характеристик в области течения и проведен их анализ.